

MRS DISTINGUISHED INVITED SPEAKER



Leveraging local structural disorder for enhanced ion transport

Michael J. Deck¹, Yan-Yan Hu^{1,2,a)}

¹Department of Chemistry and Biochemistry, Florida State University, Tallahassee, FL 32306, USA

²National High Magnetic Field Laboratory, Tallahassee, FL 32310, USA

^{a)}Address all correspondence to this author. e-mail: yhu@fsu.edu

Received: 14 February 2023; accepted: 20 April 2023; published online: 9 May 2023

Fast-ion conductors, also known as solid electrolytes, are a critical component to the development of high-performance all-solid-state batteries. Conventional lithium solid electrolytes are limited by low ionic conductivity due to high energy barriers for Li⁺ transport. Recent advancements in promoting fast-ion transport have been achieved through weakening the interaction of Li-ions with their coordinated anions via the introduction of local disorder on the atomic-, nano-, and meso-scale. Difficulty in the coherent characterization of local-entropy-enhanced ion conductors arises from the modified structural framework, which consists of highly disordered local structures within an ordered long-range network. This review outlines an experimental approach to systematically probe the relation between material structure, ion dynamics, and ion conduction, guided by solid-state NMR. Examples of our work on local-entropy-enhanced ion conductors are highlighted to encourage future studies to further optimize the properties of solid electrolytes for a wide range of technological applications.

Introduction

Lithium-ion batteries (LIBs) have quickly become ubiquitous to power consumer electronics and electric vehicles with the required energy and power density for their intended purpose. As these technologies become more advanced and widespread, the batteries that power them must improve as well. Key metrics that must be considered are the cost, energy and power density, and safe operation of the battery, which are all largely related to the materials used within the battery. Current LIBs generally consist of three main components: the anode, cathode, and electrolyte. An electric potential difference exists between the anode and cathode, with the electrolyte between them [1]. Current commercialized LIBs typically utilize a carbon host as the anode, intercalation-type transition metal oxides such as LiMO₂ (M = Co, Ni, or Mn) as the cathode, and a lithium salt such as LiPF₆ dissolved in organic solvents, e.g. ethylene carbonate/diethylene carbonate, as the electrolyte [1, 2]. Numerous studies have been conducted on optimizing the materials used to enhance the aforementioned key metrics. Notably, in nearly all essential components in batteries, including electrodes, electrolytes, composites of them, and interphases between them, their Li⁺ transport properties are shown to be a crucial factor to the

electrochemical performance. Enhanced Li⁺ transport within the electrodes and electrolyte increases the ionic conductivity and consequently gives greater utilization of the energy storage capacity and improved power performance of LIBs [2–4].

While the Li⁺ conductivity in all components of LIBs require improvement for optimal performance, this review will focus on our recent work to enhance Li⁺ conductivity within electrolytes, particularly solid electrolytes (SEs), through leveraging increased entropy in local structures and ion dynamics. With respect to current commercial LIBs, the use of SEs has emerged as an advantageous replacement for liquid electrolytes (LEs). SEs for all-solid-state batteries (ASSBs) have many advantages: they eliminate the need to use flammable solvents in LIBs for enhanced safety and reduced cost [5, 6], are compatible with high-voltage cathodes and lithium metal anode [7, 8], and allow dense packaging for increased energy density [9, 10]. The ionic conductivities of SEs can now match and even surpass that of LEs [11–13]. The recent significant enhancements in ionic conductivity have been attributed to creating a “frustrated” energy landscape via several types of disorder such as chemical, structural, and dynamical, which lead to fast-ion conduction [14].

Significant work has been done to understand the role of the long-range structural framework on ionic conductivity in SEs [15, 16]. However, the local structural environments, i.e., the solvation layer of the active cations, and their ordering also play a key role in determining ion conduction properties. In this regard, magnetic resonance techniques stand out as essential to understanding short-range structure and ion transport phenomena to provide insights into how to tune local structures for enhanced ion conduction.

Herein, a strategy for implementing local entropy to enhance Li^+ transport within SEs, guided by solid-state NMR, will be detailed. In addition, a review of our work on utilizing induced local entropy to enhance the ionic conductivity of SEs on the atomic, nano, and mesoscale will be presented using several examples.

Entropy-enhanced ion transport in different classes of electrolytes

Several classes of electrolytes exist such as LEs, polymer electrolytes, and inorganic electrolytes. Between these electrolyte classes, the mechanism of ion transport varies significantly, as shown in Figure 1. LEs in LIBs are generally comprised of lithium salts dissolved in aprotic organic solvents. The Li^+ ions are located within highly disordered solvation shells, due to the motion of the liquid solvent molecules, where Li^+ transport

occurs through co-diffusion (Li^+ ions move with the first solvation shell and the solvation shell does not change) and structure-diffusion (Li^+ ions move by exchange of solvation molecules in their first and outer solvation shells) [17–19]. In contrast, polymer electrolytes generally consist of lithium salts distributed in a polymer matrix. In comparison with LEs, there is decreased disorder surrounding the Li^+ ions due to the directional covalent bonds of the polymer. The flexibility of polymers allows for Li^+ transport through an intrachain hop (Li^+ moves along the polymer chain via exchanging a coordinating monomer for a neighboring monomer), interchain hop (Li^+ moves by exchanging several coordinating monomers at the same time), and/or through ion-polymer co-diffusion (Li^+ moves with the polymer chain without changing coordination site, dominant mechanism for low-molecular-weight polymer electrolytes) [18] [20–25]. For crystalline inorganic SEs, Li^+ ions are located within ordered anion sublattice cages (solvation cages) [26]. Ion transport occurs by Li^+ hopping through interconnected diffusion channels via vacancy sites, interstitials, or interstitial knock-offs [15, 16, 25, 27]. Importantly, for each type of hop to occur, the Li^+ ions must overcome an energy barrier, E_a , for which its magnitude can be related to the configuration entropy, $\Delta S_{\text{configuration}}$. From LEs to inorganic electrolytes, the $\Delta S_{\text{configuration}}$ decreases due to the increasingly ordered Li^+ solvation environments. As a result, in general, LEs have the highest Li^+ diffusivity ($10^{-10} \text{ m}^2/\text{s}$) [17, 28] with polymers having intermediate Li^+ diffusivity

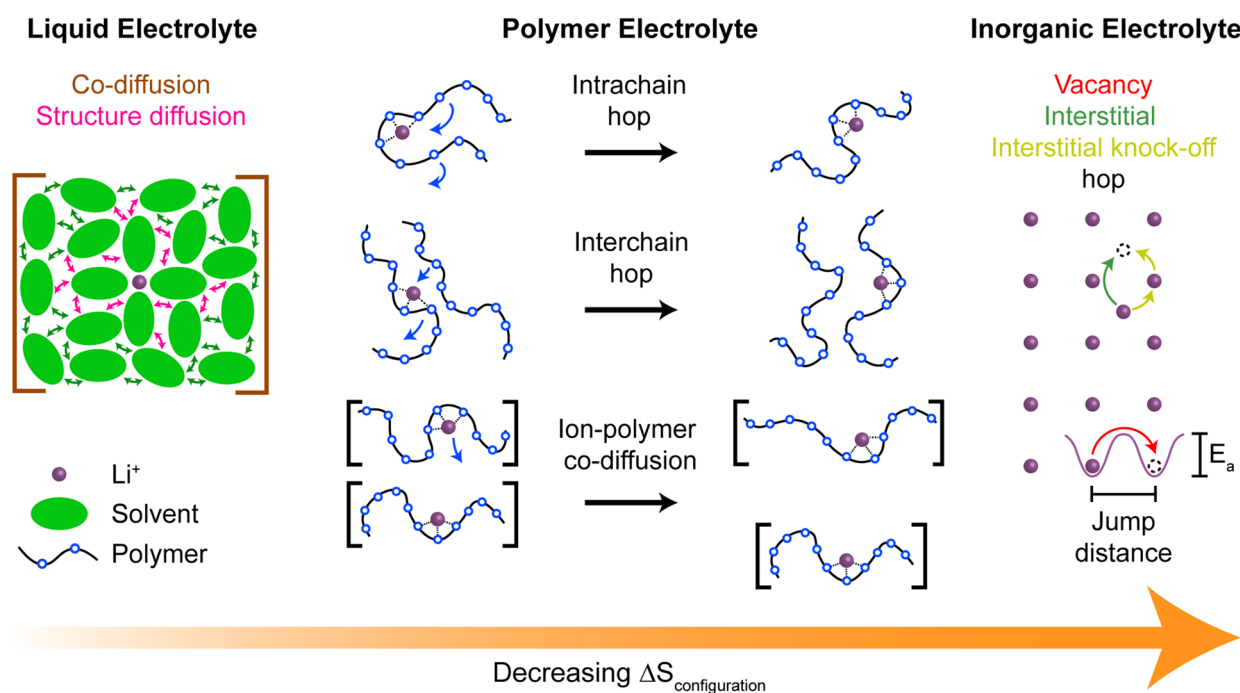


Figure 1: Li^+ transport mechanisms for liquid, polymer, and inorganic electrolytes. Liquid electrolytes utilize co-diffusion and structure diffusion. Structure diffusion is also known as solvent-exchange. Polymer electrolytes utilize intrachain hops, interchain hops, and/or ion-polymer co-diffusion. Inorganic electrolytes utilize vacancy, interstitial, and interstitial knock-off hops. Anions are excluded for clarity. Co-diffusion transport mechanisms are also known as vehicular transport mechanisms.

values (10^{-11} m²/s) [29, 30] and ceramics having the lowest (10^{-12} – 10^{-13} m²/s) [31–33]. The Li⁺ diffusivity trend coincides with the general E_a values showing a significantly lower value for LEs (0.15 – 0.25 eV) [34, 35] than polymer (0.7 – 1.4 eV) [36, 37] and ceramic electrolytes (0.15 – 0.6 eV) [33, 38, 39].

Based on these trends, it can be inferred that the local entropy of solvated active cations can be further manipulated to tune Li⁺ conduction in electrolytes. For example, within LEs, increasing local disorder using a mixture of solvents allows for increased ion dissociation and leads to a greater number of mobile ions and improvements in diffusivity and conductivity [40, 41]. Similar enhancements are seen in polymer electrolytes through the engineering of molecular channels. For example, coordinating immobile Cu²⁺ ions within cellulose fibrils widens the diffusion channels and allows for Li⁺ solvation and Li⁺ hopping along the polymer chain via a diverse group of polar functional groups [42]. The Li-ions exhibit a similar affinity to coordinate with the different oxygen-rich polar functional groups (RO•••Li, COO•••Li, and ROH/H₂O•••Li) resulting in Li-ions being able to dissociate from oxygen bonds while coordinating with others along the diffusion channel, as shown from solid-state NMR. In other words, the Li- ions are not energetically “trapped” by any of the functional groups.

Local disorder-enhanced Li⁺ conduction has also been applied to inorganic SEs to yield superionic conductors. These superionic conductors are stabilized enthalpically as well as entropically, producing a liquid-like diffusive sublattice within the crystal lattice [14]. For example, a flattened energy landscape is achieved in sulfide, oxide, and halide ceramic SEs by tuning the local ordering surrounding Li-ions [14]. Structural

distortions create a distribution of Li⁺ site energies and an energetic overlap between neighboring Li⁺ sites, which prevents Li-ions from energetically favoring one site over the neighbor site (ion frustration), thereby enhancing Li⁺ transport [14, 43–46]. The local disorder can enable new low-energy-barrier Li⁺ percolation pathways to be formed, and in some cases increases the dimensionality of Li⁺ transport (2D to 3D) [43, 44, 47]. Our findings support the theory that local disorder can be beneficial in creating superionic SE phases by creating a frustrated energy landscape [14, 43, 45] over the atomic, nano, and mesoscale. A key question is then how to systematically implement and characterize local disorder as well as how to correlate the local structure with ion conduction and dynamics.

Characterization of local structure and ion transport in solid electrolytes

Strategic development of local-entropy-enhanced ion conductors

A strategy to characterize and deploy local structural disorder to enhance ion transport has been implemented. Structure-ion conduction correlation needs to be first established – for which a suite of suitable experimental techniques is necessary (Figure 2).

First, a promising structural framework must be determined based on tunability and versatile ion transport channels. Then, functional local disorder can be engineered to promote ion conduction. A few key characteristics of disorder include the nature, the concentration, and the location. The structural framework can be described by long-range and short-range ordering. Bragg diffraction, such as in X-ray/neutron diffraction can be used to

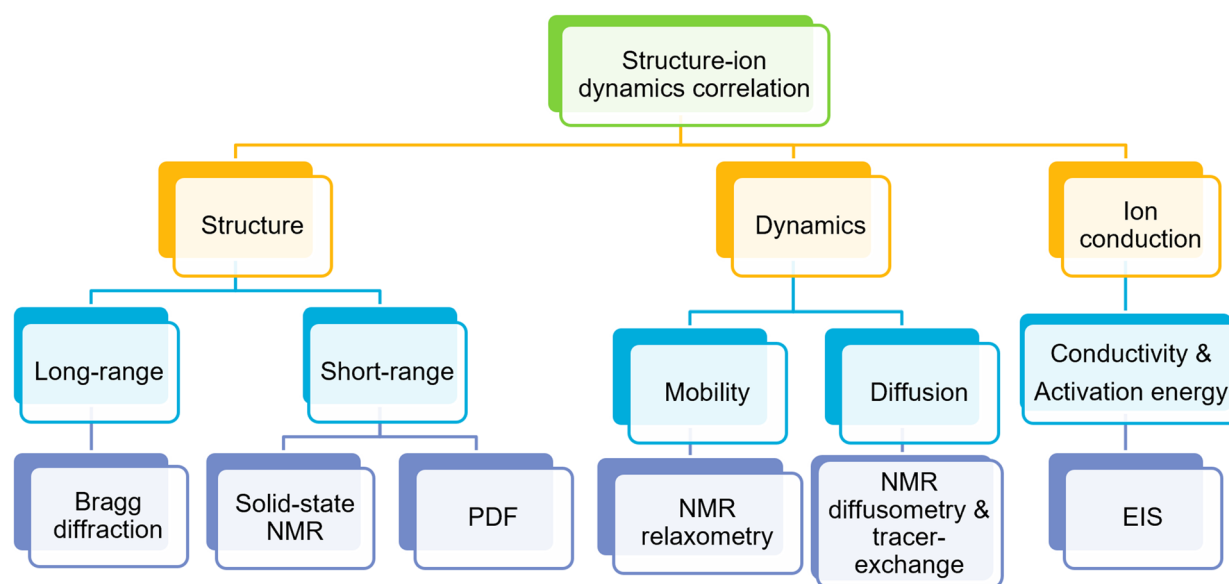


Figure 2: Characterization of structure, dynamics, and ion conduction in SEs.

determine the long-range structure [48], whereas short-range (local) structure can be studied using solid-state NMR and pair distribution function (PDF) analysis [49–52]. Intuitively, the structure and chemical composition of SEs have a large impact on the Li^+ transport. Second, the ion dynamics need to be measured. Ion mobility can be determined with NMR relaxometry [53–56], ion diffusion can be probed with NMR diffusometry [41, 55, 57–59], and ion transport pathways can be mapped out with tracer-exchange NMR [42, 60–63]. Third, on the macroscopic level, electrochemical impedance spectroscopy (EIS) is employed to measure ionic conductivity, activation energy (E_a), and dimensionality of Li^+ transport (1D, 2D, or 3D) [64, 65]. It should be noted that solid-state NMR can also determine ionic conductivity and E_a but on a shorter length scale than EIS [51, 59, 65, 66]. The information obtained on the microscopic scale should be correlated and cross-checked with macroscopic mass transport. Moreover, superionic phases detected from solid-state NMR can be isolated through synthesis optimization to improve ionic conductivity, as confirmed with EIS.

Computational screening of electrolyte structure and ion transport

Several computational techniques can be used to complement experimental studies of ion transport. For example, when introducing a certain type of disorder (chemical, structural, dynamical) into the SE, a critical question is how it affects the ion transport and stability of the structure. To address this, computational screening by calculating properties such as ionic conductivity, activation energy, ion transport pathways, thermodynamic stability, etc. is advantageous to narrow down promising synthesizable ion conductors. In brief, with respect to structure, the enthalpy of mixing (ΔH_{mix}) can be used to determine the relative thermodynamic stability of the target structure in comparison to the thermodynamically stable phases [47, 67]. For sublattice migration energy barriers and pathways, nudged elastic band (NEB) calculations can be used [68–70]. For bulk ion conduction, ab-initio molecular dynamics (AIMD) can be used to computationally determine diffusivity, activation energy, ionic conductivity, and dimensionality of Li^+ transport [47, 68, 69, 71, 72]. Lithium probability density derived from AIMD can be used to determine the interconnectivity of Li^+ diffusion pathways [47, 68, 73–75].

Compositional or structural disorder can be introduced and their effects on ion transport can be examined with computational methods. For disorder on the atomic and nanoscale, structural parameters of the pristine SE can be obtained from sources such as the Inorganic Crystal Structure Database (ICSD) [76] and/or Materials Project database [77]. Point defects are then introduced via vacancy creation or alio-/iso-valent substitution [12, 44, 47]. Density functional theory (DFT) calculations

can then be used to determine the lowest energy structures and synthesizability. The resulting modified structural parameters can be input into NEB or AIMD to calculate ion transport properties [47, 78]. For disorder on the mesoscale, such as interfaces, computations become challenging due to the extensiveness of the defects with complex compositions; however, these highly disordered systems are being pursued with advanced computational methods combining DFT, machine-learned interatomic potentials, and MD with large structural models [79–83].

Determining the state of disorder

After synthesizing the target SE with functional disorder, it is essential to experimentally determine the state of disorder achieved to correlate it with the Li^+ transport properties. Several methods can be used to probe the state of disorder. Notably, synchrotron-based techniques are commonly used for their high-energy X-ray and neutron beams. For example, with the total scattering of synchrotron X-rays or neutrons, PDF analysis can be used to determine short- and intermediate-range structural information such as bond lengths, bond angles, and coordination numbers of the atoms in the material [51, 84–86]. Another synchrotron-based technique to determine the degree of disorder is X-ray absorption spectroscopy (XAS). For example, temperature-dependent extended X-ray absorption fine structure (EXAFS) analysis is used to determine element-specific interatomic distances and the environment of atoms surrounding the absorbing atom, including their relative, static, and dynamic disorder based on the spectral oscillation decay [51, 85, 87]. In some cases, Raman spectroscopy is used for probing disorder based on Raman shift, intensity, and linewidth [88–90]. Another technique used is high-angle annular dark-field scanning transmission electron microscopy (HAADF-STEM). This technique allows for the indirect determination of disorder by observing the change in image contrast upon modifying the structural framework [91–94]. Solid-state NMR is an element-specific technique highly sensitive to local structural disorder and ion dynamics [65, 95–98], making it unique for establishing structural disorder-ion transport correlations.

Ion transport characterized by solid-state NMR

Ion transport is a complex process; it requires a repertoire of different techniques to determine relevant parameters and ensure the coherency of measurements on different time and length scales [51]. For instance, DC ionic conductivity is a macroscopic parameter often determined by EIS [51, 65, 99–101]. To understand how/why materials produce a certain DC ionic conductivity, we need to determine the

individual microscopic parameters, for which solid-state NMR is indispensable.

To fully understand the utility of solid-state NMR to study ion transport and thereby guide SE development, we must consider the variables that determine macroscopic ionic conductivity, σ , as seen in Eq. 1 [51]:

$$\sigma = \frac{1}{6} \frac{f}{H_R} \frac{cq^2}{k_B T} a^2 \nu_0 \exp\left[\frac{\Delta S}{k_B}\right] \exp\left[-\frac{\Delta H}{k_B T}\right] \quad (1)$$

where $\frac{1}{6}$ is related to 3D isotropic motion, f is the correlation factor and is defined as the ratio between the tracer diffusion coefficient, D^* , and the random diffusion coefficient, D_r ($f = \frac{D^*}{D_r}$). H_R represents the Haven ratio, which is the ratio of the tracer diffusion coefficient D^* and the long-range diffusion coefficient D_σ , $H_R = \frac{D^*}{D_\sigma}$. c represents active ion concentration, q represents the charge of the active ion, k_B represents the Boltzmann constant, T represents the absolute temperature, a represents the hopping distance between two neighboring sites, ν_0 represents the attempt frequency, ΔS represents the entropy, and ΔH represents the activation enthalpy (also known as activation energy, E_a). With a combination of computation, diffraction, solid-state NMR, and EIS, nearly all these variables can be determined. c can be estimated using pulsed-field gradient (PFG) NMR spectroscopy and EIS [51]. D^* (also known as diffusivity) can be determined from PFG NMR [41, 59, 102]. D_r can be determined from variable-temperature NMR using the Einstein–Smoluchowski relation, and D_σ is determined using EIS [51, 66, 103]. NMR relaxometry is used to measure jump frequencies and motional correlation rate using spin–lattice, T_1 , and spin–spin, T_2 , relaxation measurements [41, 53, 104]. EIS can also be used to calculate the jump frequency on a larger length scale than NMR and MD simulations can be used to calculate ν_0 [71, 105]. Jump distance can be determined from MD computations [106] or crystallographic sites from single-crystal XRD [107]. ΔS can be determined using a statistical mechanic approach [108] or from variable-temperature EIS [105]. ΔH is generally determined from variable-temperature EIS [105].

As can be seen, accurate determination of the parameters for macroscopic ionic conductivity requires several meticulously detailed experiments for each system of study, for which the time and length scale of each measurement must be carefully considered. Moreover, accurately determining ion diffusion in solids is also very challenging and often limited by a short T_2 and the existence of multiple diffusion processes [41]. A simplified experimental approach is to focus on ion transport pathways in SEs as these thermodynamic and kinetic aspects of ion transport are largely dependent on the structurally available transport pathways, as will also be discussed below with an example using tracer-exchange NMR [42, 60–63].

Inducing local entropy to enhance ion transport in solid electrolyte systems

SEs allow for local entropy to be introduced in multiple ways: chemical, structural, and dynamical [14]. The overarching effect of all three types of disorder is weakening the Li^+ interactions with the coordinated anions and causing Li^+ “frustration”. Furthermore, structural disorder can occur on the atomic, nano, or mesoscale and each should be carefully considered for the enhancement of ion transport, which will be highlighted with examples of each discussed in detail below.

Introducing local structural disorder via synthesis

Many synthesis and fabrication methods can be used to make SEs that leverage local structural disorder on the atomic, nano, and mesoscale. For introducing disorder on the atomic scale, solid-state synthesis is widely used to introduce dopants into the parent materials [109, 110]. Generally, this includes the use of a ball miller (e.g. high-energy or planetary miller) and/or hand-mixing to achieve a homogeneous mixture of precursors, which are then heated at the desired temperature and duration [12]. A slow cool down to room temperature (annealing) or fast cool down (quenching) will greatly impact the structures and properties. Quenching can allow for the stabilization of high-temperature metastable phases that may have high ionic conductivity [111]. Similarly, ball milling can also be used for mechanochemical synthesis via the milling balls colliding into the precursors in a manner that mimics quenching [110]. Depending on the system and the amount of time milled, the resulting material and properties can vary greatly and therefore should be optimized [66, 97, 109, 112, 113]. Another approach is solvent-assisted synthesis [114]. This method can allow for greater morphological control of the SE however the compatibility of the solvent must be considered. For inducing local structural disorder on the nanoscale, ball milling can be used to form structural frameworks with weakened Li^+ -anion interactions [115]. Ball milling can cause defects on the nanoscale and generate amorphous and glass–ceramic (upon subsequent heating) materials with high ionic conductivity [109, 116, 117]. Furthermore, mechanochemical milling can be used to extrinsically cause site disorder and structural frustration to produce superionic conductors [14, 86, 109, 118]. Local structural disorder on the mesoscale can be accomplished through fabricating composite SEs. For example, a ceramic or glass SE can be added to a polymer SE and cast into a film [60]. The non-uniform nature of the interface between the mixed composite components and potential reaction products cause disorder on the mesoscale and if optimized can yield improved Li^+ transport through the interfaces [60].

Disorder on the atomic scale

The argyrodite class of ceramic SEs is widely used for its tunable chemical structure and can serve as a model structural framework to probe local-entropy-enhanced ion conduction [12, 65, 74, 75, 106, 119–121]. Within the argyrodite structure, ion conduction is strongly dependent on disorder [65]. For the pristine, $\text{Li}_6\text{PS}_5\text{X}$ has a cubic structure in the F-43 m space group. Li-ions occupy the 24 g and 48 h crystallographic sites. PS_4^{3-} tetrahedra fill octahedral sites with phosphorus in 4b sites and sulfur in 16e. The remaining sulfur is in 4d sites, and halides in 4a sites [12, 121–123]. Based on our calculation, such an arrangement delivers very low Li^+ diffusivity and high E_a . Upon introducing anion disorder, we have found that S^{2-}/X^- mixing leads to significant conductivity enhancement with a reduction in E_a . For example, our work on $\text{Li}_{6-x}\text{PS}_{5-x}\text{ClBr}_x$ ($x=0.7$) has shown an ionic conductivity of 24 mS/cm at 25 °C with an E_a of 0.155 eV, which is comparable to Li^+ transport in liquids [Figure 3(a), (b)] [12]. Moreover, a longer jump distance and higher jump frequency is generated [Figure 3(b)], which contributes to the macroscopic ionic conductivity enhancement (Eq. 1). With diversifying halide species and increasing the X^- amount, we were able to achieve maximum disorder over the 4a and 4d sites via random distribution of S^{2-} , Cl^- , and Br^- over these two sites, as determined by both diffraction and solid-state NMR. The random distribution of anions causes Li-ions to redistribute among the 24 g and 48 h sites, as suggested by ^6Li NMR shifts. This leads to induced hyper-coordination and increased coordination entropy for the Li-sublattice and thereby a “frustrated” energy landscape. As a result, the Li^+ mobility increases, indicated by ^7Li T_1 relaxation measurements. Therefore, we have created compositions that allow the maximum mixed-site occupancy, with nearly zero

energy penalty, i.e., ΔH_{mix} . This is a noticeable improvement in Li^+ transport when compared to our work on the less disordered $\text{Li}_{6-x}\text{PS}_{5-x}\text{Cl}_{1+x}$ ($x=0.7$), which has an ionic conductivity of 17 mS/cm at 25 °C and an E_a of 0.22 eV [75], and $\text{Li}_{6-x}\text{PS}_{5-x}\text{Br}_{1+x}$ ($x=0.7$), which achieves an ionic conductivity of 11 mS/cm at 25 °C with an E_a of 0.18 eV [74]—further demonstrating the benefits of local disorder on the atomic scale to enhance ion transport.

Disorder on the nanoscale

An example of disorder on the nanoscale can be seen in the $1.4\text{Li}_3\text{PO}_4\text{-LiI}$ binary system [115]. Li_3PO_4 has two common polymorphs: A low-temperature $\beta\text{-Li}_3\text{PO}_4$ phase (Pmn2₁) and a high-temperature $\gamma\text{-Li}_3\text{PO}_4$ phase (Pnma) that is reported to irreversibly form at >340 °C [124–126]. The difference in structure between the two polymorphs is that $\beta\text{-Li}_3\text{PO}_4$ has PO_4^{3-} tetrahedra aligned in the same direction while $\gamma\text{-Li}_3\text{PO}_4$ has PO_4^{3-} tetrahedra oriented in opposite directions, with a $\sim 1.4\%$ volume expansion occurring for the $\beta \rightarrow \gamma\text{-Li}_3\text{PO}_4$ transformation. The comparison of ionic conductivities is shown in Figure 4(a). Notably, crystalline $\beta\text{-Li}_3\text{PO}_4$ has a room-temperature ionic conductivity of 10^{-17} S/cm which increases to 10^{-9} S/cm for the glassy $\beta\text{-Li}_3\text{PO}_4$ phase, illustrating the effect of poly-anion disorder on Li^+ transport. Moreover, in comparison to $\beta\text{-Li}_3\text{PO}_4$, $\gamma\text{-Li}_3\text{PO}_4$ has a decreased E_a [Figure 4(b)]. To further leverage the nanoscale disorder, LiI can be mechanochemically introduced into the sublattice to create a solid solution. This process forms a glassy mixed-anion framework of PO_4^{3-} and I^- , yielding bulk $\text{Li}_{3.06}\text{PO}_4\text{I}_{0.06}$ with glassy- $\text{Li}_4\text{PO}_4\text{I}$ at the interface. The computed ionic conductivity of glassy- $\text{Li}_4\text{PO}_4\text{I}$ shows an even further increased value of 10^{-4} S/cm and decreased E_a as

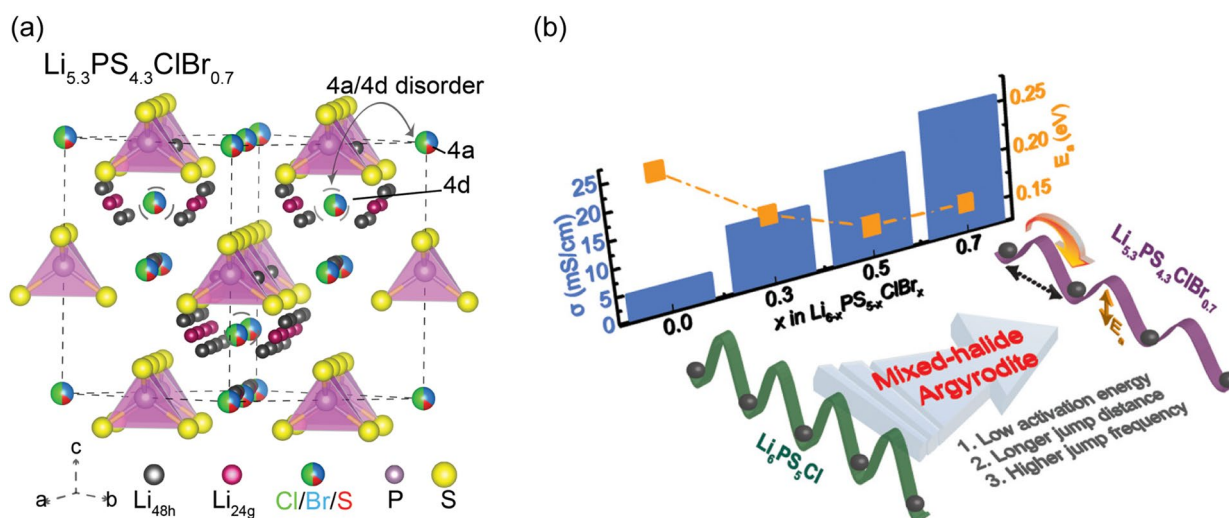


Figure 3: (a) Average crystal structure of mixed-halide argyrodite $\text{Li}_{6-x}\text{PS}_{5-x}\text{ClBr}_x$ ($x=0.7$) derived from Bragg diffraction refinement. (b) Induced local entropy in the mixed-halide argyrodite SE enables lower E_a , longer jump distance, and higher jump frequency—all contributing to increased ionic conductivity in comparison to the pristine argyrodite. Adapted with permission from Patel et al. [12] Copyright 2021 American Chemical Society.

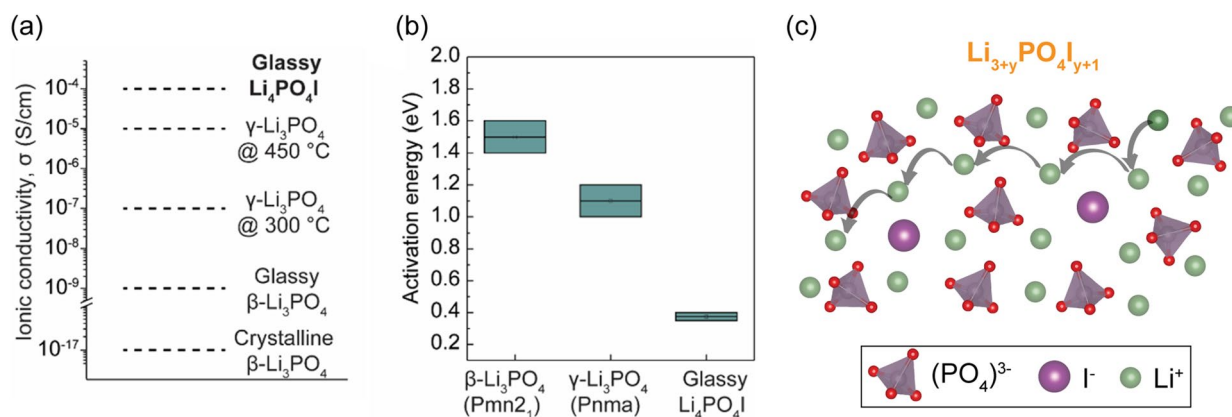


Figure 4: (a) Experimental ionic conductivities of Li_3PO_4 polymorphs and computed ionic conductivity of glassy- $\text{Li}_4\text{PO}_4\text{I}$ from AIMD simulations. (b) Corresponding activation energies of Li_3PO_4 polymorphs and glassy- $\text{Li}_4\text{PO}_4\text{I}$. (c) Illustration of enhanced ion transport within $\text{Li}_3\text{PO}_4\text{-LiI}$. Adapted with permission from Patel et al. [115] Copyright 2022 Elsevier.

seen in Figures 4(a), (b). ^7Li T_1 values indicate increased Li^+ mobility for $\text{Li}_{3.06}\text{PO}_4\text{I}_{0.06}$ and glassy- $\text{Li}_4\text{PO}_4\text{I}$ in comparison to the pristine precursors (Li_3PO_4 and LiI). Tracer-exchange NMR showed that the glassy- $\text{Li}_4\text{PO}_4\text{I}$ phase is responsible for the enhanced ionic conductivity, whereby the Li -ions readily jump from interacting with PO_4^{3-} to I^- anions, with equal resident time on them, suggested by a weighted ^6Li NMR shift. This is the ideal case for fast-ion conduction, as the equal opportunity of Li -ions interacting with all the anions suggests that Li -ions are not “trapped” by any of the anions. The summary of these results is shown in Figure 4(c), illustrating that disorder on the nanoscale causes an interruption of the PO_4^{3-} network by I^- , which prevents the trapping of Li^+ by either type of anions. Applying to both crystalline and glassy materials, a balanced interaction between all anions and Li -ions is required to prevent local trapping and promote fast-ion conduction.

Disorder on the mesoscale

Disorder on the mesoscale can be exemplified in composite electrolytes. Composite electrolytes aim to combine the advantages of polymer (flexible) and ceramic electrolytes (high conductivity). However, the significant hurdle of achieving a commercially viable ionic conductivity of greater than 1 mS/cm at room temperature with a low E_a remains an area of active research. One promising strategy to leverage disorder in these composite systems is to create a polymer-ceramic interface that can conduct Li -ions. The interfaces formed are inherently disordered as they contain an inhomogeneous combination of the polymer, ceramic, lithium salt, solvent, and possible new phases. Our group has fabricated several composite electrolyte systems that validate this strategy, contingent upon an optimized composition [60, 63]. Notably, the ion transport pathway can be tuned depending on the composition, and the lowest

energy pathway is not always through the interface [62]. One example can be seen in a ceramic polymer thin film electrolyte composed of $\text{Li}_{10}\text{GeP}_2\text{S}_{12}$ -poly(ethylene oxide)-lithium bis(trifluoromethanesulfonyl)imide (LGPS-PEO(LiTFSI)) [Figure 5(a)] [60]. Solid-state NMR enables us to identify the components of the composite including the interface. Upon varying the wt% of LGPS, EIS measurements show a maximum conductivity is achieved when the interface is also maximized [Figure 5(b)]. Furthermore, the optimized composite shows an E_a in between that of the pure PEO(LiTFSI) electrolyte and LGPS [Figure 5(c)]. For the conductivity-optimized combination of the PEO polymer, LiTFSI, and LGPS, tracer-exchange NMR indeed shows that the Li -ions go through the interface during conduction.

Conclusion and future prospects

Ion transport is a critical factor to consider among the anode, cathode, and electrolyte in the development of ASSBs. For SEs, the use of local disorder on the atomic, nano, and mesoscale has been shown to greatly improve ion dynamics and ionic conductivity. Solid-state NMR is an important tool to help guide efforts to further leverage local entropy through a combination of local structure, mobility, and diffusion measurements, as well as ion transport pathway determination.

In summary, we surveyed the phenomenon of entropy-enhanced ion conduction across multiple length scales. Despite all the differences in these materials, the common aspect is that the Li^+ —anion interaction is weakened by introducing local disorder, thereby promoting enhanced Li^+ transport. It is pertinent to clarify that increasing $\Delta S_{\text{configuration}}$ does not always produce thermodynamically stable superionic phases as the ΔH_{mix} must also be considered. Moreover, increased $\Delta S_{\text{configuration}}$ does not

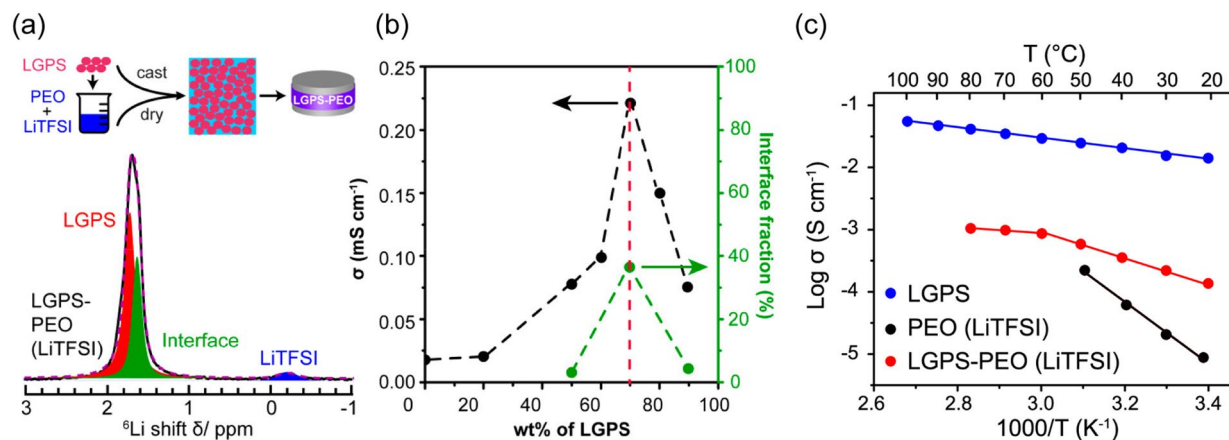


Figure 5: Ceramic polymer thin film electrolyte composed of $\text{Li}_{10}\text{GeP}_2\text{S}_{12}$ -poly(ethylene oxide)-lithium bis(trifluoromethanesulfonyl)imide (a) Top: schematic of preparation process to make the hybrid thin film and symmetric cell used for galvanostatic cycling. Bottom: ^6Li NMR spectrum of the LGPS-PEO (LiTFSI) 70 wt% LGPS hybrid thin film with spectral fitting to show the LGPS, interface, and LiTFSI components. (b) Ionic conductivity and interface fraction as a function of wt% of LGPS in LGPS-PEO (LiTFSI) (9:1). (c) Arrhenius plots of LGPS, PEO (LiTFSI) (9:1), and 70 wt% LGPS-PEO (LiTFSI) (9:1). Adapted with permission from Zheng et al. [60] Copyright 2019 American Chemical Society.

always give improved ionic conductivity as many other important factors contribute to enhancing macroscopic ionic conductivity such as the connectivity of long-range Li^+ pathways, as described above. Situating the right local disorder in long-range structures conducive to fast ion conduction is key. Therefore, detailed studies on the nature of local disorder and its correlation with ion transport are essential. The strategy described in this review to enhance ionic conductivity can also be used more broadly in other areas of materials research as superionic conduction is not only crucial to battery performance but to other technologies such as sensors [127–129], fuel cells [130–132], etc. In other systems, such as hybrid perovskites [133–135], ion migration is detrimental to their stable performance. The reverse strategy can be adopted to immobilize ions.

Funding

The authors acknowledge the support from the National Science Foundation under grant no. DMR-1847038 and from the NSF MRSEC program (NSF DMR-1720139).

Data availability

Data available on request from authors.

Declarations

Conflict of interest On behalf of all authors, the corresponding author states that there is no conflict of interest.

References

1. J.-K. Park, *Principles and Applications of Lithium Secondary Batteries* (Wiley, New York, 2012). <https://doi.org/10.1002/9783527650408>
2. Y. Saito, Ion transport in solid medium-evaluation of ionic mobility for design of ion transport pathways in separator and gel electrolyte. *Membranes* (Basel) (2021). <https://doi.org/10.3390/membranes11040277>
3. B.W. Byles, N.K.R. Palapati, A. Subramanian, E. Pomerantseva, The role of electronic and ionic conductivities in the rate performance of tunnel structured manganese oxides in Li-ion batteries. *APL Mater.* 4(4), 46108 (2016). <https://doi.org/10.1063/1.4948272>
4. E. Hosseinzadeh, J. Marco, P. Jennings, The impact of multi-layered porosity distribution on the performance of a lithium ion battery. *Appl. Math. Model.* 61, 107–123 (2018). <https://doi.org/10.1016/j.apm.2018.04.001>
5. A. Manthiram, X. Yu, S. Wang, Lithium battery chemistries enabled by solid-state electrolytes. *Nat. Rev. Mater.* 2, 16103 (2017). <https://doi.org/10.1038/natrevmats.2016.103>
6. T. Ye, L. Li, Y. Zhang, Recent progress in solid electrolytes for energy storage devices. *Adv. Funct. Mater.* 30(29), 2000077 (2020). <https://doi.org/10.1002/adfm.202000077>
7. A.M. Nolan, Y. Liu, Y. Mo, Solid-state chemistries stable with high-energy cathodes for lithium-ion batteries. *ACS Energy Lett.* 4(10), 2444–2451 (2019). <https://doi.org/10.1021/acsenenergylett.9b01703>

8. S. Kim, J.-S. Kim, L. Miara, Y. Wang, S.-K. Jung, S.Y. Park, Z. Song, H. Kim, M. Badding, J. Chang, V. Roev, G. Yoon, R. Kim, J.-H. Kim, K. Yoon, D. Im, K. Kang, High-energy and durable lithium metal batteries using garnet-type solid electrolytes with tailored lithium-metal compatibility. *Nat. Commun.* **13**(1), 1883 (2022). <https://doi.org/10.1038/s41467-022-29531-x>
9. T. Placke, R. Kloepsch, S. Dühnen, M. Winter, Lithium ion, lithium metal, and alternative rechargeable battery technologies: the odyssey for high energy density. *J. Solid State Electrochem.* **21**(7), 1939–1964 (2017). <https://doi.org/10.1007/s10008-017-3610-7>
10. Y. Huang, B. Shao, F. Han, Solid-state batteries: an introduction. In *Solid State Batteries Volume 1: Emerging Materials and Applications*; ACS Symposium Series; American Chemical Society, 2022; Vol. 1413, p 1. <https://doi.org/10.1021/bk-2022-1413.ch001>.
11. J.C. Bachman, S. Muy, A. Grimaud, H.H. Chang, N. Pour, S.F. Lux, O. Paschos, F. Maglia, S. Lupart, P. Lamp, L. Giordano, Y. Shao-Horn, Inorganic solid-state electrolytes for lithium batteries: mechanisms and properties governing ion conduction. *Chem. Rev.* (2016). <https://doi.org/10.1021/acs.chemrev.5b00563>
12. S.V. Patel, S. Banerjee, H. Liu, P. Wang, P.-H. Chien, X. Feng, J. Liu, S.P. Ong, Y.-Y. Hu, Tunable lithium-ion transport in mixed-halide argyrodites $\text{Li}_{6-x}\text{PS}_{5-x}\text{ClBr}_x$: an unusual compositional space. *Chem. Mater.* **33**(4), 1435–1443 (2021). <https://doi.org/10.1021/acs.chemmater.0c04650>
13. Y. Kato, S. Hori, T. Saito, K. Suzuki, M. Hirayama, A. Mitsui, M. Yonemura, H. Iba, R. Kanno, High-power all-solid-state batteries using sulfide superionic conductors. *Nat. Energy* **1**(4), 1–3 (2016). <https://doi.org/10.1038/nenergy.2016.30>
14. B.C. Wood, J.B. Varley, K.E. Kweon, P. Shea, A.T. Hall, A. Grieder, M. Ward, V.P. Aguirre, D. Rigling, E. Lopez Ventura, C. Stancill, N. Adelstein, Paradigms of frustration in superionic solid electrolytes. *Philos. Trans. R. Soc. A* **379**(2211), 20190467 (2021). <https://doi.org/10.1098/rsta.2019.0467>
15. X. He, Y. Zhu, Y. Mo, Origin of fast ion diffusion in super-ionic conductors. *Nat. Commun.* **8**(1), 15893 (2017). <https://doi.org/10.1038/ncomms15893>
16. B. Zhang, R. Tan, L. Yang, J. Zheng, K. Zhang, S. Mo, Z. Lin, F. Pan, Mechanisms and properties of ion-transport in inorganic solid electrolytes. *Energy Storage Mater.* **10**, 139–159 (2018). <https://doi.org/10.1016/j.ensm.2017.08.015>
17. O. Borodin, G.D. Smith, LiTFSI structure and transport in ethylene carbonate from molecular dynamics simulations. *J. Phys. Chem. B* **110**(10), 4971–4977 (2006). <https://doi.org/10.1021/jp056249q>
18. C.Y. Son, Z.-G. Wang, Ion transport in small-molecule and polymer electrolytes. *J. Chem. Phys.* **153**(10), 100903 (2020). <https://doi.org/10.1063/5.0016163>
19. K. Dokko, D. Watanabe, Y. Ugata, M.L. Thomas, S. Tsuzuki, W. Shinoda, K. Hashimoto, K. Ueno, Y. Umabayashi, M. Watanabe, Direct evidence for Li ion hopping conduction in highly concentrated sulfolane-based liquid electrolytes. *J. Phys. Chem. B* **122**(47), 10736–10745 (2018). <https://doi.org/10.1021/acs.jpcc.8b09439>
20. Q. Zhang, K. Liu, F. Ding, X. Liu, Recent advances in solid polymer electrolytes for lithium batteries. *Nano Res.* **10**(12), 4139–4174 (2017). <https://doi.org/10.1007/s12274-017-1763-4>
21. L. Yue, J. Ma, J. Zhang, J. Zhao, S. Dong, Z. Liu, G. Cui, L. Chen, All solid-state polymer electrolytes for high-performance lithium ion batteries. *Energy Storage Mater.* **5**, 139–164 (2016). <https://doi.org/10.1016/j.ensm.2016.07.003>
22. D. Golodnitsky, E. Strauss, E. Peled, S. Greenbaum, On order and disorder in polymer electrolytes. *J. Electrochem. Soc.* **162**(14), A2551 (2015). <https://doi.org/10.1149/2.0161514jes>
23. G. Rollo-Walker, N. Malic, X. Wang, J. Chiefari, M. Forsyth, Development and progression of polymer electrolytes for batteries: influence of structure and chemistry. *Polymers* (2021). <https://doi.org/10.3390/polym13234127>
24. Z. Xue, D. He, X. Xie, Poly(ethylene oxide)-based electrolytes for lithium-ion batteries. *J. Mater. Chem. A* **3**(38), 19218–19253 (2015). <https://doi.org/10.1039/C5TA03471J>
25. H. Yang, N. Wu, Ionic conductivity and ion transport mechanisms of solid-state lithium-ion battery electrolytes: a review. *Energy Sci. Eng.* **10**(5), 1643–1671 (2022). <https://doi.org/10.1002/ese3.1163>
26. D.J. Siegel, L. Nazar, Y.-M. Chiang, C. Fang, N.P. Balsara, Establishing a unified framework for ion solvation and transport in liquid and solid electrolytes. *Trends Chem.* **3**(10), 807–818 (2021). <https://doi.org/10.1016/j.trechm.2021.06.004>
27. M. Park, X. Zhang, M. Chung, G.B. Less, A.M. Sastry, A review of conduction phenomena in Li-ion batteries. *J. Power Sources* **195**(24), 7904–7929 (2010). <https://doi.org/10.1016/j.jpowsour.2010.06.060>
28. K. Hayamizu, Direct relations between ion diffusion constants and ionic conductivity for lithium electrolyte solutions. *Electrochim. Acta* **254**, 101–111 (2017). <https://doi.org/10.1016/j.electacta.2017.09.051>
29. G. Foran, D. Mankovsky, N. Verdier, D. Lepage, A. Pr  b  , D. Aym  -Perrot, M. Doll  , The impact of absorbed solvent on the performance of solid polymer electrolytes for use in solid-state lithium batteries. *iScience* **23**, 101597 (2020). <https://doi.org/10.1016/j.isci.2020.101597>
30. D.J. Brooks, B.V. Merinov, W.A.I.I.I. Goddard, B. Kozinsky, J. Mailoa, Atomistic description of ionic diffusion in PEO–LiTFSI: effect of temperature, molecular weight, and ionic concentration. *Macromolecules* **51**(21), 8987–8995 (2018). <https://doi.org/10.1021/acs.macromol.8b01753>
31. R.H. Brugge, R.J. Chater, J.A. Kilner, A. Aguadero, Experimental determination of Li diffusivity in LLZO using isotopic

- exchange and FIB-SIMS. *J. Phys. Energy* **3**(3), 34001 (2021). <https://doi.org/10.1088/2515-7655/abe2f7>
32. K. Hayamizu, Y. Terada, K. Kataoka, J. Akimoto, T. Haishi, Relationship between Li^+ diffusion and ion conduction for single-crystal and powder garnet-type electrolytes studied by ^7Li PGSE NMR spectroscopy. *Phys. Chem. Chem. Phys.* **21**(42), 23589–23597 (2019). <https://doi.org/10.1039/C9CP04714J>
 33. F.M. Pesci, A. Bertei, R.H. Brugge, S.P. Emge, A.K.O. Hekselman, L.E. Marbella, C.P. Grey, A. Agüero, Establishing ultralow activation energies for lithium transport in garnet electrolytes. *ACS Appl. Mater. Interfaces* **12**(29), 32806–32816 (2020). <https://doi.org/10.1021/acsami.0c08605>
 34. Y. Domi, H. Usui, T. Hirotsawa, K. Sugimoto, T. Nakano, A. Ando, H. Sakaguchi, Impact of low temperatures on the lithiation and delithiation properties of Si-based electrodes in ionic liquid electrolytes. *ACS Omega* (2022). <https://doi.org/10.1021/acsomega.2c00947>
 35. T.R. Jow, S.A. Delp, J.L. Allen, J.-P. Jones, M.C. Smart, Factors limiting Li^+ charge transfer kinetics in Li-ion batteries. *J. Electrochem. Soc.* **165**(2), A361 (2018). <https://doi.org/10.1149/2.1221802jes>
 36. B.N. Choi, J.H. Yang, Y.S. Kim, C.-H. Chung, Effect of morphological change of copper-oxide fillers on the performance of solid polymer electrolytes for lithium-metal polymer batteries. *RSC Adv.* **9**(38), 21760–21770 (2019). <https://doi.org/10.1039/C9RA03555A>
 37. V. St-Onge, M. Cui, S. Rochon, J.-C. Daigle, J.P. Claverie, Reducing crystallinity in solid polymer electrolytes for lithium-metal batteries via statistical copolymerization. *Commun. Mater.* **2**(1), 83 (2021). <https://doi.org/10.1038/s43246-021-00187-2>
 38. G. Sahu, E. Rangasamy, J. Li, Y. Chen, K. An, N. Dudney, C. Liang, A high-conduction Ge substituted Li_3AsS_4 solid electrolyte with exceptional low activation energy. *J. Mater. Chem. A* **2**(27), 10396–10403 (2014). <https://doi.org/10.1039/C4TA01243G>
 39. Z. Deng, B. Radhakrishnan, S. Ong, Rational composition optimization of the lithium-rich $\text{Li}_3\text{OCl}_{1-x}\text{Br}_x$ anti-perovskite superionic conductors. *Chem. Mater.* **27**, 150508153056007 (2015). <https://doi.org/10.1021/acs.chemmater.5b00988>
 40. Ishii, S.; Yamada, S.; Ishikawa, T.; Fujinami, T.; Hayashi, Y.; Otsuka, H.; Ito, K.; Kubo, Y.; Saito, M. Enhancement of Bifunctional Effect of NO_3^- Anion By Using Glyme-Based Dual Solvent Electrolytes for Li-Air Batteries. In *ECS Meeting Abstracts*; IOP Publishing, 2018; p 347. Doi: <https://doi.org/10.1149/MA2018-02/5/347>.
 41. K.S. Han, J.D. Bazak, Y. Chen, T.R. Graham, N.M. Washton, J.Z. Hu, V. Murugesan, K.T. Mueller, Pulsed field gradient nuclear magnetic resonance and diffusion analysis in battery research. *Chem. Mater.* **33**(22), 8562–8590 (2021). <https://doi.org/10.1021/acs.chemmater.1c02891>
 42. C. Yang, Q. Wu, W. Xie, X. Zhang, A. Brozena, J. Zheng, M.N. Garaga, B.H. Ko, Y. Mao, S. He, Y. Gao, P. Wang, M. Tyagi, F. Jiao, R. Briber, P. Albertus, C. Wang, S. Greenbaum, Y.-Y. Hu, A. Isogai, M. Winter, K. Xu, Y. Qi, L. Hu, Copper-coordinated cellulose ion conductors for solid-state batteries. *Nature* **598**(7882), 590–596 (2021). <https://doi.org/10.1038/s41586-021-03885-6>
 43. M. Botros, J. Janek, Embracing disorder in solid-state batteries. *Science* (80-) **378**(6626), 1273–1274 (2022). <https://doi.org/10.1126/science.adf3383>
 44. Y. Zeng, B. Ouyang, J. Liu, Y.-W. Byeon, Z. Cai, L.J. Miara, Y. Wang, G. Ceder, High-entropy mechanism to boost ionic conductivity. *Science* (80-) **378**(6626), 1320–1324 (2022). <https://doi.org/10.1126/science.abq1346>
 45. D. Di Stefano, A. Miglio, K. Robeyns, Y. Filinchuk, M. Lechartier, A. Senyshyn, H. Ishida, S. Spannenberger, D. Prutsch, S. Lunghammer, D. Rettenwander, M. Wilkening, B. Roling, Y. Kato, G. Hautier, Superionic diffusion through frustrated energy landscape. *Chemistry* **5**(9), 2450–2460 (2019). <https://doi.org/10.1016/j.chempr.2019.07.001>
 46. L. Zhou, A. Assoud, A. Shyamsunder, A. Huq, Q. Zhang, P. Hartmann, J. Kulisch, L.F. Nazar, An entropically stabilized fast-ion conductor: $\text{Li}_{3.25}[\text{Si}_{0.25}\text{P}_{0.75}]\text{S}_4$. *Chem. Mater.* **31**(19), 7801–7811 (2019). <https://doi.org/10.1021/acs.chemmater.9b00657>
 47. S. Banerjee, M.L. Holekevi Chandrappa, S.P. Ong, Role of critical oxygen concentration in the $\beta\text{-Li}_3\text{PS}_{4-x}\text{O}_x$ solid electrolyte. *ACS Appl. Energy Mater.* **5**(1), 35–41 (2022). <https://doi.org/10.1021/acsaem.1c03795>
 48. P.-C. Tsai, S. Mair, J. Smith, D.M. Halat, P.-H. Chien, K. Kim, D. Zhang, Y. Li, L. Yin, J. Liu, S.H. Lapidus, J.A. Reimer, N.P. Balsara, D.J. Siegel, Y.-M. Chiang, Double paddle-wheel enhanced sodium ion conduction in an antiperovskite solid electrolyte. *Adv. Energy Mater.* (2022). <https://doi.org/10.1002/aenm.202203284>
 49. S. Kmiec, A. Joyce, D. Bayko, S.W. Martin, Glass formation and structure of melt quenched mixed oxy-sulfide $\text{Na}_4\text{P}_2\text{S}_{7-x}\text{O}_x$ glasses for $0 \leq x \leq 5$. *J. Non Cryst. Solids* **534**, 119776 (2020). <https://doi.org/10.1016/j.jnoncrysol.2019.119776>
 50. S. Shiotani, K. Ohara, H. Tsukasaka, S. Mori, R. Kanno, Pair distribution function analysis of sulfide glassy electrolytes for all-solid-state batteries: understanding the improvement of ionic conductivity under annealing condition. *Sci. Rep.* **7**(1), 6972 (2017). <https://doi.org/10.1038/s41598-017-07086-y>
 51. Y. Gao, A.M. Nolan, P. Du, Y. Wu, C. Yang, Q. Chen, Y. Mo, S.-H. Bo, Classical and emerging characterization techniques for investigation of ion transport mechanisms in crystalline fast ionic conductors. *Chem. Rev.* **120**(13), 5954–6008 (2020). <https://doi.org/10.1021/acs.chemrev.9b00747>
 52. X. Li, M. Deck, Y.-Y. Hu, Solid-state NMR and EPR characterization of transition-metal oxides for electrochemical energy

- storage. In *Transition Metal Oxides for Electrochemical Energy Storage*; 2022; pp 299–318. <https://doi.org/10.1002/9783527817252.ch12>.
53. A. Kuhn, M. Kunze, P. Sreeraj, H.-D. Wiemhöfer, V. Thangadurai, M. Wilkening, P. Heitjans, NMR relaxometry as a versatile tool to study Li ion dynamics in potential battery materials. *Solid State Nucl. Magn. Reson.* **42**, 2–8 (2012). <https://doi.org/10.1016/j.ssnmr.2012.02.001>
 54. F.F. Stewart, J.F. Stebbins, E.S. Peterson, I. Farnan, S.O. Dunham, E. Adams, P.W. Jennings, Mobility and relaxation determinations of lithium in lithium aluminate ceramics using solid-state NMR spectroscopy. *Chem. Mater.* **7**(2), 363–367 (1995). <https://doi.org/10.1021/cm00050a020>
 55. D.J. Morales, S. Greenbaum, NMR investigations of crystalline and glassy solid electrolytes for lithium batteries: a brief review. *Int. J. Mol. Sci.* (2020). <https://doi.org/10.3390/ijms21093402>
 56. S. Munoz, S. Greenbaum, Review of recent nuclear magnetic resonance studies of ion transport in polymer electrolytes. *Membranes* (Basel). (2018). <https://doi.org/10.3390/membranes8040120>
 57. K. Szutkowski, D. Tubacka, P. Florczak, D. Kruk, Long-range Li-Ion 3D diffusion in the high-temperature hexagonal phase of LiBH₄ studied by ⁷Li pulsed field gradient NMR and MD simulations. *J. Phys. Chem. C* **126**(37), 15936–15943 (2022). <https://doi.org/10.1021/acs.jpcc.2c03658>
 58. N.K. Jayakody, C.C. Fraenza, S.G. Greenbaum, D. Ashby, B.S. Dunn, NMR relaxometry and diffusometry analysis of dynamics in ionic liquids and ionogels for use in lithium-ion batteries. *J. Phys. Chem. B* **124**(31), 6843–6856 (2020). <https://doi.org/10.1021/acs.jpcc.0c02755>
 59. S. Harm, A.-K. Hatz, I. Moudrakovski, R. Eger, A. Kuhn, C. Hoch, B.V. Lotsch, Lesson learned from NMR: characterization and ionic conductivity of LGPS-like Li₇SiPS₈. *Chem. Mater.* **31**(4), 1280–1288 (2019). <https://doi.org/10.1021/acs.chemmater.8b04051>
 60. J. Zheng, P. Wang, H. Liu, Y.-Y. Hu, Interface-enabled ion conduction in Li₁₀GeP₂S₁₂-poly(ethylene oxide) hybrid electrolytes. *ACS Appl. Energy Mater.* **2**(2), 1452–1459 (2019). <https://doi.org/10.1021/acsaem.8b02008>
 61. X. Feng, P.-H. Chien, S. Patel, J. Zheng, M. Immediato-Scuotto, Y. Xin, I. Hung, Z. Gan, Y.-Y. Hu, Synthesis and characterizations of highly conductive and stable electrolyte Li₁₀P₃S₁₂I. *Energy Storage Mater.* **22**, 397–401 (2019). <https://doi.org/10.1016/j.ensm.2019.07.047>
 62. J. Zheng, M. Tang, Y.-Y. Hu, Lithium ion pathway within Li₇La₃Zr₂O₁₂-polyethylene oxide composite electrolytes. *Angew. Chem. Int. Ed.* **55**(40), 12538–12542 (2016). <https://doi.org/10.1002/anie.201607539>
 63. T. Yang, J. Zheng, Q. Cheng, Y.-Y. Hu, C.K. Chan, Composite polymer electrolytes with Li₇La₃Zr₂O₁₂ garnet-type nanowires as ceramic fillers: mechanism of conductivity enhancement and role of doping and morphology. *ACS Appl. Mater. Interfaces* **9**(26), 21773–21780 (2017). <https://doi.org/10.1021/acsaami.7b03806>
 64. D.L. Sidebottom, Colloquium: understanding ion motion in disordered solids from impedance spectroscopy scaling. *Rev. Mod. Phys.* **81**(3), 999–1014 (2009). <https://doi.org/10.1103/RevModPhys.81.999>
 65. I. Hanghofer, M. Brinek, S.L. Eisbacher, B. Bitschnau, M. Volck, V. Hennige, I. Hanzu, D. Rettenwander, H.M.R. Wilkening, Substitutional disorder: structure and ion dynamics of the argyrodites Li₆PS₅Cl, Li₆PS₅Br and Li₆PS₅I. *Phys. Chem. Chem. Phys.* **21**(16), 8489–8507 (2019). <https://doi.org/10.1039/C9CP00664H>
 66. M. Gombotz, H.M.R. Wilkening, Fast Li ion dynamics in the mechanothesized nanostructured form of the solid electrolyte Li₃yBr₆. *ACS Sustain. Chem. Eng.* **9**(2), 743–755 (2021). <https://doi.org/10.1021/acssuschemeng.0c06694>
 67. S.-L. Shang, Z. Yu, Y. Wang, D. Wang, Z.-K. Liu, Origin of outstanding phase and moisture stability in a Na₃P_{1-x}As₂S₄ superionic conductor. *ACS Appl. Mater. Interfaces* **9**(19), 16261–16269 (2017). <https://doi.org/10.1021/acsaami.7b03606>
 68. H. Fang, P. Jena, Argyrodite-Type advanced lithium conductors and transport mechanisms beyond paddle-wheel effect. *Nat. Commun.* **13**(1), 2078 (2022). <https://doi.org/10.1038/s41467-022-29769-5>
 69. X. He, Y. Zhu, A. Epstein, Y. Mo, Statistical variances of diffusional properties from ab initio molecular dynamics simulations. *npj Comput. Mater.* **4**(1), 18 (2018). <https://doi.org/10.1038/s41524-018-0074-y>
 70. A. Baktash, J.C. Reid, Q. Yuan, T. Roman, D.J. Searles, Shaping the future of solid-state electrolytes through computational modeling. *Adv. Mater.* **32**(18), 1908041 (2020). <https://doi.org/10.1002/adma.201908041>
 71. N.J.J. de Klerk, E. van der Maas, M. Wagemaker, Analysis of diffusion in solid-state electrolytes through MD simulations, improvement of the Li-ion conductivity in β-Li₃PS₄ as an example. *ACS Appl. Energy Mater.* **1**(7), 3230–3242 (2018). <https://doi.org/10.1021/acsaem.8b00457>
 72. Y. Zhang, X. He, Z. Chen, Q. Bai, A.M. Nolan, C.A. Roberts, D. Banerjee, T. Matsunaga, Y. Mo, C. Ling, Unsupervised discovery of solid-state lithium ion conductors. *Nat. Commun.* **10**(1), 5260 (2019). <https://doi.org/10.1038/s41467-019-13214-1>
 73. C. Wang, J. Liang, J.T. Kim, X. Sun, Prospects of halide-based all-solid-state batteries: from material design to practical application. *Sci. Adv.* **8**(36), eadc9516 (2022). <https://doi.org/10.1126/sciadv.adc9516>
 74. P. Wang, H. Liu, S. Patel, X. Feng, P.-H. Chien, Y. Wang, Y.-Y. Hu, Fast ion conduction and its origin in Li_{6-x}PS_{5-x}Br_{1+x}. *Chem. Mater.* **32**(9), 3833–3840 (2020). <https://doi.org/10.1021/acs.chemmater.9b05331>

75. X. Feng, P.-H. Chien, Y. Wang, S. Patel, P. Wang, H. Liu, M. Immediato-Scuotto, Y.-Y. Hu, Enhanced ion conduction by enforcing structural disorder in Li-deficient argyrodites $\text{Li}_{6-x}\text{PS}_{5-x}\text{Cl}_{1+x}$. *Energy Storage Mater.* **30**, 67–73 (2020). <https://doi.org/10.1016/j.ensm.2020.04.042>
76. G. Bergerhoff, R. Hundt, R. Sievers, I.D. Brown, The inorganic crystal structure data base. *J. Chem. Inf. Comput. Sci.* **23**(2), 66–69 (1983). <https://doi.org/10.1021/ci00038a003>
77. A. Jain, S.P. Ong, G. Hautier, W. Chen, W.D. Richards, S. Dacek, S. Cholia, D. Gunter, D. Skinner, G. Ceder, K.A. Persson, Commentary: the materials project: a materials genome approach to accelerating materials innovation. *APL Mater.* **1**(1), 11002 (2013). <https://doi.org/10.1063/1.4812323>
78. G. Ceder, S.P. Ong, Y. Wang, Predictive modeling and design rules for solid electrolytes. *MRS Bull.* **43**(10), 746–751 (2018). <https://doi.org/10.1557/mrs.2018.210>
79. K. Choudhary, B. DeCost, C. Chen, A. Jain, F. Tavazza, R. Cohn, C.W. Park, A. Choudhary, A. Agrawal, S.J.L. Billinge, E. Holm, S.P. Ong, C. Wolverton, Recent advances and applications of deep learning methods in materials science. *npj Comput. Mater.* **8**(1), 59 (2022). <https://doi.org/10.1038/s41524-022-00734-6>
80. C. Chen, Y. Zuo, W. Ye, X. Li, Z. Deng, S.P. Ong, A critical review of machine learning of energy materials. *Adv. Energy Mater.* **10**(8), 1903242 (2020). <https://doi.org/10.1002/aenm.201903242>
81. C.W. Park, M. Kornbluth, J. Vandermause, C. Wolverton, B. Kozinsky, J.P. Mailoa, Accurate and scalable graph neural network force field and molecular dynamics with direct force architecture. *npj Comput. Mater.* **7**(1), 73 (2021). <https://doi.org/10.1038/s41524-021-00543-3>
82. L. Ward, C. Wolverton, Atomistic calculations and materials informatics: a review. *Curr. Opin. Solid State Mater. Sci.* **21**(3), 167–176 (2017). <https://doi.org/10.1016/j.cossms.2016.07.002>
83. Y. Zuo, C. Chen, X. Li, Z. Deng, Y. Chen, J. Behler, G. Csányi, A.V. Shapeev, A.P. Thompson, M.A. Wood, S.P. Ong, Performance and cost assessment of machine learning interatomic potentials. *J. Phys. Chem. A* **124**(4), 731–745 (2020). <https://doi.org/10.1021/acs.jpca.9b08723>
84. M.W. Terban, S.J.L. Billinge, Structural analysis of molecular materials using the pair distribution function. *Chem. Rev.* **122**(1), 1208–1272 (2022). <https://doi.org/10.1021/acs.chemrev.1c00237>
85. A.P. Black, A. Sorrentino, F. Fauth, I. Yousef, L. Simonelli, C. Frontera, A. Ponrouch, D. Tonti, M.R. Palacin, Synchrotron radiation based operando characterization of battery materials. *Chem. Sci.* **14**(7), 1641–1665 (2023). <https://doi.org/10.1039/d2sc04397a>
86. R. Schlem, S. Muy, N. Prinz, A. Banik, Y. Shao-Horn, M. Zobel, W.G. Zeier, Mechanochemical synthesis: a tool to tune cation site disorder and ionic transport properties of Li_3MCl_6 ($M = \text{Y}, \text{Er}$) superionic conductors. *Adv. Energy Mater.* **10**(6), 1903719 (2020). <https://doi.org/10.1002/aenm.201903719>
87. W. Olszewski, M. Ávila Pérez, C. Marini, E. Paris, X. Wang, T. Iwao, M. Okubo, A. Yamada, T. Mizokawa, N.L. Saini, L. Simonelli, Temperature dependent local structure of Na_xCoO_2 cathode material for rechargeable sodium-ion batteries. *J. Phys. Chem. C* **120**(8), 4227–4232 (2016). <https://doi.org/10.1021/acs.jpcc.5b10885>
88. V. Varade, G.V. Honnavar, P. Anjaneyulu, K.P. Ramesh, R. Menon, Probing disorder and transport properties in polypyrrole thin-film devices by impedance and raman spectroscopy. *J. Phys. D* **46**(36), 365306 (2013). <https://doi.org/10.1088/0022-3727/46/36/365306>
89. J.S. Weaving, A. Lim, J. Millichamp, T.P. Neville, D. Ledwoch, E. Kendrick, P.F. McMillan, P.R. Shearing, C.A. Howard, D.J.L. Brett, Elucidating the Sodiation Mechanism in Hard Carbon by Operando Raman Spectroscopy. *ACS Appl. Energy Mater.* **3**(8), 7474–7484 (2020). <https://doi.org/10.1021/acsaem.0c00867>
90. S. Pérez-Villar, P. Lanz, H. Schneider, P. Novák, Characterization of a model solid electrolyte interphase/carbon interface by combined in situ Raman/Fourier transform infrared microscopy. *Electrochim. Acta* **106**, 506–515 (2013). <https://doi.org/10.1016/j.electacta.2013.05.124>
91. Y. Pei, Q. Chen, M. Wang, P. Zhang, Q. Ren, J. Qin, P. Xiao, L. Song, Y. Chen, W. Yin, X. Tong, L. Zhen, P. Wang, C.-Y. Xu, A medium-entropy transition metal oxide cathode for high-capacity lithium metal batteries. *Nat. Commun.* **13**(1), 6158 (2022). <https://doi.org/10.1038/s41467-022-33927-0>
92. X. Hu, C.A.J. Fisher, S. Kobayashi, Y.H. Ikuhara, Y. Fujiwara, K. Hoshikawa, H. Moriwake, K. Kohama, H. Iba, Y. Ikuhara, Structural changes and their effect on Li-ion conductivity upon quenching of $\text{La}_{(1-x)}\text{Li}_x\text{NbO}_3$ solid electrolytes. *Acta Mater.* **156**, 379–388 (2018). <https://doi.org/10.1016/j.actamat.2018.06.006>
93. Z. Wang, D. Santhanagopalan, W. Zhang, F. Wang, H.L. Xin, K. He, J. Li, N. Dudney, Y.S. Meng, In situ STEM-EELS observation of nanoscale interfacial phenomena in all-solid-state batteries. *Nano Lett.* **16**(6), 3760–3767 (2016). <https://doi.org/10.1021/acs.nanolett.6b01119>
94. S. Li, Z. Yao, J. Zheng, M. Fu, J. Cen, S. Hwang, H. Jin, A. Orlov, L. Gu, S. Wang, Z. Chen, D. Su, Direct observation of defect-aided structural evolution in a nickel-rich layered cathode. *Angew. Chem. Int. Ed.* **59**(49), 22092–22099 (2020). <https://doi.org/10.1002/anie.202008144>
95. Y. García, L. Porcarelli, H. Zhu, M. Forsyth, D. Mecerreyes, L.A. O'Dell, Probing disorder and dynamics in composite electrolytes of an organic ionic plastic crystal and lithium functionalised acrylic polymer nanoparticles. *J. Magn. Reson. Open* **14–15**, 100095 (2023). <https://doi.org/10.1016/j.jmro.2023.100095>

96. D.H.S. Tan, E.A. Wu, H. Nguyen, Z. Chen, M.A.T. Marple, J.-M. Doux, X. Wang, H. Yang, A. Banerjee, Y.S. Meng, Elucidating reversible electrochemical redox of $\text{Li}_6\text{PS}_5\text{Cl}$ solid electrolyte. *ACS Energy Lett.* **4**(10), 2418–2427 (2019). <https://doi.org/10.1021/acsenergylett.9b01693>
97. T. Famprikis, Ö.U. Kudu, J.A. Dawson, P. Canepa, F. Fauth, E. Suard, M. Zbiri, D. Dambournet, O.J. Borkiewicz, H. Bouyanfif, S.P. Emge, S. Cretu, J.-N. Chotard, C.P. Grey, W.G. Zeier, M.S. Islam, C. Masquelier, Under pressure: mechanochemical effects on structure and ion conduction in the sodium-ion solid electrolyte Na_3PS_4 . *J. Am. Chem. Soc.* **142**(43), 18422–18436 (2020). <https://doi.org/10.1021/jacs.0c06668>
98. K. Chen, A practical review of NMR lineshapes for Spin-1/2 and quadrupolar nuclei in disordered materials. *Int. J. Mol. Sci.* (2020). <https://doi.org/10.3390/ijms21165666>
99. A. Düvel, M. Wilkening, R. Uecker, S. Wegner, V. Šepelák, P. Heitjans, Mechanothesized nanocrystalline BaLiF_3 : the impact of grain boundaries and structural disorder on ionic transport. *Phys. Chem. Chem. Phys.* **12**(37), 11251–11262 (2010). <https://doi.org/10.1039/C004530F>
100. P. Vadhva, J. Hu, M.J. Johnson, R. Stocker, M. Braglia, D.J.L. Brett, A.J.E. Rennie, Electrochemical impedance spectroscopy for all-solid-state batteries: theory, methods and future outlook. *ChemElectroChem* **8**(11), 1930–1947 (2021). <https://doi.org/10.1002/celec.202100108>
101. S. Kmiec, M. Olson, M. Kenney, S.W. Martin, Interpretation of the Na^+ ionic conductivity in $\text{Na}_4\text{P}_2\text{S}_{7-x}\text{O}_x$ mixed oxy-sulfide glasses: effects of oxygen doping. *Chem. Mater.* **34**(21), 9479–9491 (2022). <https://doi.org/10.1021/acs.chemmater.2c01934>
102. M.T. Chowdhury, R. Takekawa, Y. Iwai, N. Kuwata, J. Kawamura, Lithium ion diffusion in $\text{Li} \beta$ -alumina single crystals measured by pulsed field gradient NMR spectroscopy. *J. Chem. Phys.* **140**(12), 4509 (2014). <https://doi.org/10.1063/1.4869347>
103. A. Rudy, A. Mironenko, V. Naumov, A. Novozhilova, A. Skundin, I. Fedorov, Determination of diffusion coefficients of lithium in solid electrolyte LiPON . *Batteries* (2021). <https://doi.org/10.3390/batteries7020021>
104. K. Hogrefe, N. Minafra, W.G. Zeier, H.M.R. Wilkening, Tracking ions the direct way: long-range Li^+ dynamics in the Thio-LISICON family Li_4MCh_4 ($\text{M} = \text{Sn, Ge}$; $\text{Ch} = \text{S, Se}$) as probed by ^7Li NMR relaxometry and ^7Li spin-alignment echo NMR. *J. Phys. Chem. C* **125**(4), 2306–2317 (2021). <https://doi.org/10.1021/acs.jpcc.0c10224>
105. B.E. Francisco, C.R. Stoldt, J.-C. M'Peko, Energetics of ion transport in NASICON-type electrolytes. *J. Phys. Chem. C* **119**(29), 16432–16442 (2015). <https://doi.org/10.1021/acs.jpcc.5b03286>
106. N.J.J. de Klerk, I. Rosłoń, M. Wagemaker, Diffusion mechanism of Li argyrodite solid electrolytes for Li -ion batteries and prediction of optimized halogen doping: the effect of Li vacancies, halogens, and halogen disorder. *Chem. Mater.* **28**(21), 7955–7963 (2016). <https://doi.org/10.1021/acs.chemmater.6b03630>
107. A. Kuhn, O. Gerbig, C. Zhu, F. Falkenberg, J. Maier, B.V. Lotsch, A New Ultrafast Superionic Li -Conductor: Ion Dynamics in $\text{Li}_{11}\text{Si}_2\text{PS}_{12}$ and Comparison with Other Tetragonal LGPS-Type Electrolytes. *Phys. Chem. Chem. Phys.* **16**(28), 14669–14674 (2014). <https://doi.org/10.1039/C4CP02046D>
108. S. Palakkathodi Kammampata, H. Yamada, T. Ito, R. Paul, V. Thangadurai, The activation entropy for ionic conduction and critical current density for Li charge transfer in novel garnet-type $\text{Li}_{6.5}\text{La}_{2.9}\text{A}_{0.1}\text{Zr}_{1.4}\text{Ta}_{0.6}\text{O}_{12}$ ($\text{A} = \text{Ca, Sr, Ba}$) solid electrolytes. *J. Mater. Chem. A* **8**(5), 2581–2590 (2020). <https://doi.org/10.1039/C9TA12193E>
109. A. Banik, T. Famprikis, M. Ghidui, S. Ohno, M.A. Kraft, W.G. Zeier, On the underestimated influence of synthetic conditions in solid ionic conductors. *Chem. Sci.* **12**(18), 6238–6263 (2021). <https://doi.org/10.1039/d0sc06553f>
110. T. Famprikis, P. Canepa, J.A. Dawson, M.S. Islam, C. Masquelier, Fundamentals of inorganic solid-state electrolytes for batteries. *Nat. Mater.* **18**(12), 1278–1291 (2019). <https://doi.org/10.1038/s41563-019-0431-3>
111. K. Takada, M. Osada, N. Ohta, T. Inada, A. Kajiyama, H. Sasaki, S. Kondo, M. Watanabe, T. Sasaki, Lithium ion conductive oxy-sulfide, $\text{Li}_3\text{PO}_4\text{-Li}_3\text{PS}_4$. *Solid State Ionics* **176**(31), 2355–2359 (2005). <https://doi.org/10.1016/j.ssi.2005.03.023>
112. L. Schweiger, K. Hogrefe, B. Gadermaier, J.L.M. Rupp, H.M.R. Wilkening, Ionic conductivity of nanocrystalline and amorphous $\text{Li}_{10}\text{GeP}_2\text{S}_{12}$: the detrimental impact of local disorder on ion transport. *J. Am. Chem. Soc.* **144**(22), 9597–9609 (2022). <https://doi.org/10.1021/jacs.1c13477>
113. B. Gadermaier, B. Stanje, A. Wilkening, I. Hanzu, P. Heitjans, H.M.R. Wilkening, Glass in two forms: heterogeneous electrical relaxation in nanoglassy petalite. *J. Phys. Chem. C* **123**(15), 10153–10162 (2019). <https://doi.org/10.1021/acs.jpcc.9b01423>
114. Z. Liu, W. Fu, E.A. Payzant, X. Yu, Z. Wu, N.J. Dudney, J. Kiggins, K. Hong, A.J. Rondinone, C. Liang, Anomalous high ionic conductivity of nanoporous $\beta\text{-Li}_3\text{PS}_4$. *J. Am. Chem. Soc.* **135**(3), 975–978 (2013). <https://doi.org/10.1021/ja3110895>
115. S.V. Patel, E. Truong, H. Liu, Y. Jin, B.L. Chen, Y. Wang, L. Miara, R. Kim, Y.-Y. Hu, Interrupted anion-network enhanced Li^+ -ion conduction in $\text{Li}_{3+y}\text{PO}_4\text{I}_y$. *Energy Storage Mater.* **51**, 88–96 (2022). <https://doi.org/10.1016/j.ensm.2022.06.026>
116. H. Morimoto, H. Yamashita, M. Tatsumisago, T. Minami, Mechanochemical synthesis of new amorphous materials of $60\text{Li}_2\text{S}\cdot 40\text{SiS}_2$ with high lithium ion conductivity. *J. Am. Ceram. Soc.* **82**(5), 1352–1354 (1999). <https://doi.org/10.1111/j.1151-2916.1999.tb01923.x>
117. K. Kanazawa, S. Yubuchi, C. Hotehama, M. Otoyama, S. Shimono, H. Ishibashi, Y. Kubota, A. Sakuda, A. Hayashi, M. Tatsumisago, Mechanochemical synthesis and characterization of metastable hexagonal Li_4SnS_4 solid electrolyte. *Inorg. Chem.*

- 57(16), 9925–9930 (2018). <https://doi.org/10.1021/acs.inorgchem.8b01049>
118. Gombotz, M.; Wilkening, A.; Wilkening, H. M. R. Lithium Ion Transport in Micro- and Nanocrystalline Lithium Sulphide Li_2S . *2022*, 77 (6), 397–404. doi:<https://doi.org/10.1515/znb-2022-0013>.
119. B.J. Morgan, Mechanistic origin of superionic lithium diffusion in anion-disordered $\text{Li}_6\text{PS}_5\text{X}$ argyrodites. *Chem. Mater.* **33**(6), 2004–2018 (2021). <https://doi.org/10.1021/acs.chemmater.0c03738>
120. L. Zhou, N. Minafra, W.G. Zeier, L.F. Nazar, Innovative approaches to Li-argyrodite solid electrolytes for all-solid-state lithium batteries. *Acc. Chem. Res.* **54**(12), 2717–2728 (2021). <https://doi.org/10.1021/acs.accounts.0c00874>
121. A. Gautam, M. Sadowski, M. Ghidui, N. Minafra, A. Senyshyn, K. Albe, W.G. Zeier, Engineering the site-disorder and lithium distribution in the lithium superionic argyrodite $\text{Li}_6\text{PS}_5\text{Br}$. *Adv. Energy Mater.* **11**(5), 2003369 (2021). <https://doi.org/10.1002/aenm.202003369>
122. M.A. Kraft, S.P. Culver, M. Calderon, F. Böcher, T. Krauskopf, A. Senyshyn, C. Dietrich, A. Zevalkink, J. Janek, W.G. Zeier, Influence of lattice polarizability on the ionic conductivity in the lithium superionic argyrodites $\text{Li}_6\text{PS}_5\text{X}$ (X = Cl, Br, I). *J. Am. Chem. Soc.* **139**(31), 10909–10918 (2017). <https://doi.org/10.1021/jacs.7b06327>
123. I. Hanghofer, B. Gadermaier, H.M.R. Wilkening, Fast rotational dynamics in argyrodite-type $\text{Li}_6\text{PS}_5\text{X}$ (X: Cl, Br, I) as seen by ^{31}P nuclear magnetic relaxation—on cation-anion coupled transport in thiophosphates. *Chem. Mater.* **31**(12), 4591–4597 (2019). <https://doi.org/10.1021/acs.chemmater.9b01435>
124. C. Ibarra-Ramírez, M.E. Villafuerte-Castrejón, A.R. West, Continuous, martensitic nature of the transition $\beta \rightarrow \gamma$ Li_3PO_4 . *J. Mater. Sci.* **20**(3), 812–816 (1985). <https://doi.org/10.1007/BF00585719>
125. N.D. Lepley, N.A.W. Holzwarth, Y.A. Du, Structures, Li^+ mobilities, and interfacial properties of solid electrolytes Li_3PS_4 and Li_3PO_4 from first principles. *Phys. Rev. B* **88**(10), 104103 (2013). <https://doi.org/10.1103/PhysRevB.88.104103>
126. Y.A. Du, N.A.W. Holzwarth, Mechanisms of Li^+ diffusion in crystalline γ - and β - Li_3PO_4 electrolytes from first principles. *Phys. Rev. B* **76**(17), 174302 (2007). <https://doi.org/10.1103/PhysRevB.76.174302>
127. S. Xu, J.-X. Yu, H. Guo, S. Tian, Y. Long, J. Yang, L. Zhang, Force-induced ion generation in zwitterionic hydrogels for a sensitive silent-speech sensor. *Nat. Commun.* **14**(1), 219 (2023). <https://doi.org/10.1038/s41467-023-35893-7>
128. L. Shi, T. Zhu, G. Gao, X. Zhang, W. Wei, W. Liu, S. Ding, Highly stretchable and transparent ionic conducting elastomers. *Nat. Commun.* **9**(1), 2630 (2018). <https://doi.org/10.1038/s41467-018-05165-w>
129. J. Wang, B. Wu, P. Wei, S. Sun, P. Wu, Fatigue-free artificial ionic skin toughened by self-healable elastic nanomesh. *Nat. Commun.* **13**(1), 4411 (2022). <https://doi.org/10.1038/s41467-022-32140-3>
130. S. Fop, K.S. McCombie, E.J. Wildman, J.M.S. Skakle, J.T.S. Irvine, P.A. Connor, C. Savaniu, C. Ritter, A.C. Mclaughlin, High oxide ion and proton conductivity in a disordered hexagonal perovskite. *Nat. Mater.* **19**(7), 752–757 (2020). <https://doi.org/10.1038/s41563-020-0629-4>
131. B. Wang, B. Zhu, S. Yun, W. Zhang, C. Xia, M. Afzal, Y. Cai, Y. Liu, Y. Wang, H. Wang, Fast ionic conduction in semiconductor $\text{CeO}_{2-\delta}$ electrolyte fuel cells. *NPG Asia Mater.* **11**(1), 51 (2019). <https://doi.org/10.1038/s41427-019-0152-8>
132. X. Su, Z. Pan, L. An, Ion transport characteristics in membranes for direct formate fuel cells. *Front. Chem.* (2020). <https://doi.org/10.3389/fchem.2020.00765>
133. D. Moia, J. Maier, Ion transport, defect chemistry, and the device physics of hybrid perovskite solar cells. *ACS Energy Lett.* **6**(4), 1566–1576 (2021). <https://doi.org/10.1021/acsenerylett.1c00227>
134. X. Yan, W. Fan, F. Cheng, H. Sun, C. Xu, L. Wang, Z. Kang, Y. Zhang, Ion migration in hybrid perovskites: classification, identification, and manipulation. *Nano Today* **44**, 101503 (2022). <https://doi.org/10.1016/j.nantod.2022.101503>
135. W. Zhu, S. Wang, X. Zhang, A. Wang, C. Wu, F. Hao, Ion migration in organic-inorganic hybrid perovskite solar cells: current understanding and perspectives. *Small* **18**(15), 2105783 (2022). <https://doi.org/10.1002/smll.202105783>

Publisher's Note Springer Nature remains neutral with regard to jurisdictional claims in published maps and institutional affiliations.

Springer Nature or its licensor (e.g. a society or other partner) holds exclusive rights to this article under a publishing agreement with the author(s) or other rightsholder(s); author self-archiving of the accepted manuscript version of this article is solely governed by the terms of such publishing agreement and applicable law.